17th World Conference on Earthquake Engineering, 17WCEE

Sendai, Japan - September 13th to 18th 2020

A UNIFIED COMPUTATIONAL FRAMEWORK FOR FLUID-SOLID COUPLING IN MARINE EARTHQUAKE ENGINEERING

S. L. CHEN[(1)], J. R. SHEN[(2)], S. L. CHENG[(3)], J. SUN[(4)]

[(1)] *Nanjing, Nanjing University of Aeronautics and Astronautics, iemcsl@nuaa.edu.cn*
[(2)] *Nanjing, Nanjing University of Aeronautics and Astronautics, 18362963750@163.com*
[(3)] *Nanjing, Nanjing University of Aeronautics and Astronautics, chengshulin@nuaa.edu.cn*
[(4)] *Nanjing, Nanjing University of Aeronautics and Astronautics, 1047854825@qq.com*

Abstract

The simulation of seismic wavefield at seafloor and ocean acoustic field involve the coupling between seawater, saturated seabed, elastic bedrock and structure. That means, we target simulation where several types of equations are involved such as fluid, solid and saturated porous media equation. The conventional method for this fluid-solid-saturated porous media interaction problem is to use exsisting solvers of different equations and coupling method, which needs data mapping, communication and coupling algorithm between different solvers. Here, we present an alternative method, in which the coulping between different solvers is avoided. In fact, when porosity equals to one and zero, the saturated porous media is reduced to fluid and solid respectively, so we can use the porous media equation to describe the ideal fluid and solid, and the coupling between porous media, solid and fluid turns to the coupling between porous media with different porosity. Based on this idea, firstly the Biot's equations are approximated by Galerkin scheme and the explicit lumped-mass FEM is chosen, that are well suited to parallel computation. Then considering the conditions of coupling on the irregular interface between porous media with different porosity, by solving the normal and tangential interface forces, the coupled algorithm is derived, which is proved to be suitable for the coupling between fluid, solid and saturated porous media. Thus, the coupling problem between fluid, solid and saturated porous media can be brought into a unified framework, in which only the solver of saturated porous media is used. The three-dimensional parallel code for this proposed method is programed. To demonstrate the validity and feasibility of our method, we calculate the cases of a plane P wave vertically incident onto basin-like seabed, and compare our numerical results with those obtained by reflection/transmission matrix method for elastic seabed case. In general, the waveforms calculated by the two methods match well. And the waveforms for elastic seabed case and elastic saturated seabed case are compared.

Keywords: fluid-solid coupling, saturated porous medium, marine earthquake engineering, explicit lumped-mass finite element method, transmitting boundary

1. Introduction

For marine seismic surveys, forward modeling of seismic waves is required. In the seismic analysis of marine engineering structures, submarine ground motion is also required as the input of structural analysis. In addition, in the acoustic simulation of the ocean, the influence of the elastic sea floor and terrain also must be considered. In these areas, when it is necessary to study the dynamic response of a certain sea area, due to the presence of seawater, seismoacoustic scattering is involved, and it is affected by surrounding media. We call this problem the near-field seismoacoustic scattering problem in the sea area.

When the sea area is layered horizontally, the problem can be solved by the transfer matrix method. Okamoto and Takenaka[1] used the reflection / transmission matrix method to consider the fluid-solid interface conditions, and simulated the seismoacoustic scattering of the two-dimensional irregular fluid-solid interface when the P-SV wave was incident. However, this method is only suitable for terrains with gentle slopes. For steep terrains, it will lead to calculation instability. Utilizing the characteristics of boundary element method suitable for steep terrain, and the characteristics of global matrix propagator with less memory requirements in the simulation of multi-layer media, Qian and Yamanaka[1] extended the global matrix propagator, considered the fluid-solid interface conditions, and combined the boundary element method with the global matrix propagator method to simulate the seismoacoustic scattering of a two-dimensional irregular fluid-solid interface when P-SV waves are incident. Chen Shaolin et al.[3] used the Thomson-Haskell transfer matrix method to analyze the response of a horizontally stratified seawater-saturated seabed-bedrock system when P-SV waves were incident.

For complex seafloor topography, numerical methods such as finite difference method, boundary element method, finite element method, and spectral element method are generally used, and artificial boundary conditions are used to simulate the effects of infinite domains. Nakamura et al.[4] used a finite difference method to simulate seismoacoustic scattering. In order to meet the conditions of the fluid-solid interface, a second-order approximation was used for the equations near the interface, and a fourth-order approximation was used for the rest. They also simulated the seismic wave propagation of the Suruga Bay earthquake in 2009, and studied the effects of the submarine topography and seawater layer. The results show that the submarine topography has a greater impact on the amplitude and duration of the coda wave, and the seawater layer has a greater impact on the coda wave amplitude. Komatitsch et al.[5] considered the continuous normal velocity and continuous stress at the interface between seawater and bedrock to establish the integral weak form of the coupled equilibrium equation. They also obtained spectral element simulation methods of submarine seismic waves through spectral element discrete and explicit Newmark time integration. In marine acoustics, the parabolic equation (PE) method is widely used to consider the influence of submarine topography on sound wave propagation (Collins et al.[6], Tang et al.[7]). This method can quickly establish a long-range sound field, but it is difficult to consider irregular and complex terrain on the sea floor. Murphy et al.[8] used the finite element method to simulate the ocean sound field. Compared with the parabolic equation method, this method can calculate the effects of the full wave field and the complex topography of the ocean floor, but it is less efficient and ignores the shear effect of the elastic medium on the ocean floor.

The above methods all regard the seabed as elastic dry bedrock. When the sea floor is regarded as a saturated porous medium[9,10], the mutual coupling among fluids, solids, and saturated porous media[11,12] is very complicated. One solution is to discretize the sonic equation of the fluid and the equation of the solid or saturated porous medium, and consider the interface conditions by the Lagrangian multiplier method (Komatitsch et al. [5], Murphy et al.[8], Li Weihua et al.[13]) to get dynamic equation and solve it, which is usually called the monolithic method. Another solution is the partitioned method[14-22]. This method analyzes fluids and solids by different solvers, and then couples them at each time step through the interface coupling algorithm. If the monolithic method is used to solve the problem of seismoacoustic scattering, it is necessary to combine the wave equations of seawater, bedrock, and saturated porous media, which makes it difficult to implement this method by programming. If the partitioned method is adopted, seawater, bedrock, and saturated porous media can be analyzed by independent solvers, and then interface coupling is performed through data exchange, which is very inconvenient. Theoretically, solid and fluid media are special cases of saturated porous media with porosities of 0 and 1, respectively. The above couplings can all be described in the saturated porous media theoretical system. Based on this, Chen Shaolin et al.[23] established a unified calculation framework for the coupling problem between seawater, bedrock, and saturated porous media, avoiding the inconvenience of the monolithic method and the partition method.

Based on a unified computing framework, this paper develops a numerical simulation technique for near-field fluctuations in the sea area. This technique takes the free field obtained by the transfer matrix method as an input, simulates an infinite region by transmitting artificial boundaries, and uses a unified calculation framework for fluid-solid coupling in the inner domain. These methods provide techniques for seismic wave field simulation of complex media and complex terrain in the sea. In this paper, an example of a basin-shaped depression on the sea floor is used to verify the effectiveness of the method, and further analysis of seismoacoustic scattering in a saturated sea floor situation.

2. Basic theory

This paper selects the model mentioned in [24]. The vector representation of the basic differential equation of the model is as follows:

Solid-phase equilibrium equation for saturated porous media

$$\mathbf{L}_s^T\boldsymbol{\sigma}' - (1-\beta)\mathbf{L}_w^T P + b(\dot{\mathbf{U}} - \dot{\mathbf{u}}) = (1-\beta)\rho_s\ddot{\mathbf{u}} \tag{1}$$

Liquid equilibrium equation for saturated porous media

$$-\beta\mathbf{L}_w^T P + b(\dot{\mathbf{u}} - \dot{\mathbf{U}}) = \beta\rho_w\ddot{\mathbf{U}} \tag{2}$$

Compatibility equation (considering initial pore pressure and initial body strain as zero)

$$\tau = -\beta P = E_w[\beta e^w + (1-\beta)e^s] \tag{3}$$

Where $\mathbf{L}_s$ and $\mathbf{L}_w$ are differential operator matrices, $\boldsymbol{\sigma}'$ is the effective stress vector, τ is the average pore pressure, which is positive when under tension. P is the pore water pressure, which is positive when under compression. $\mathbf{U}$ and $\mathbf{u}$ respectively represent the displacement vectors of the liquid and solid phases, $\dot{\mathbf{U}}$, $\dot{\mathbf{u}}$ are the velocity, and $\ddot{\mathbf{U}}$, $\ddot{\mathbf{u}}$ are the acceleration. ρ_s and ρ_w are the density of the solid and liquid phases, respectively. β is the porosity, $b=\beta^2\mu_0/k_0$, k_0 is fluid permeability coefficient, μ_0 is the kinematic viscosity coefficient, E_w is the bulk modulus of the fluid, e^s and e^w respectively represent the volume strain of the solid and liquid phases. It can be known from the equation that when the porosity ratio is 1, it can degenerate into the ideal fluid equation, and when the porosity ratio is 0, it can degenerate into the elastic wave equation. Therefore, fluids, elastic solids, and saturated porous media can be uniformly described by the general saturated porous media ($0 \le \beta \le 1$) equation. The only difference between these materials is the material parameters. The problem of seismic wave propagation in the sea area can be described by the general saturated porous media equation, and the area of interest is calculated as shown in Figure 1.

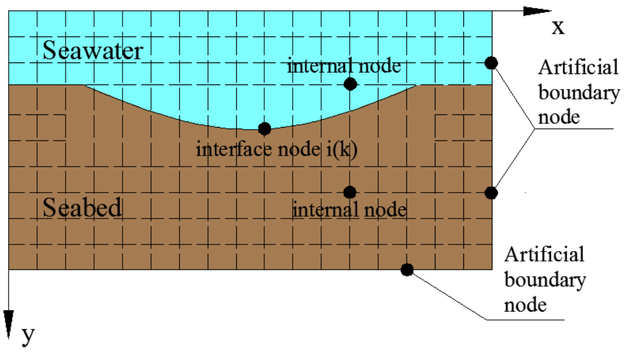

Fig.1 Schematic diagram of seawater-bedrock interaction analysis model

2.1 Wave field input

On the boundaries of the calculation area (except for free surfaces), artificial boundaries (as shown in Figure 1) need to be set up to simulate the effects of infinite domains. At the boundary, we assume that the medium is layered horizontally. Due to the damping of the medium and the boundary is far from the area we care about, this assumption has little effect on the response of the area we care about. Thus, we can use a transfer matrix method to obtain the response of a horizontally layered medium under plane wave input (free field, as shown in Figure 2), and use it as an input to the problem of seismoacoustic scattering when a complex interface is involved. For details, please refer to [3].

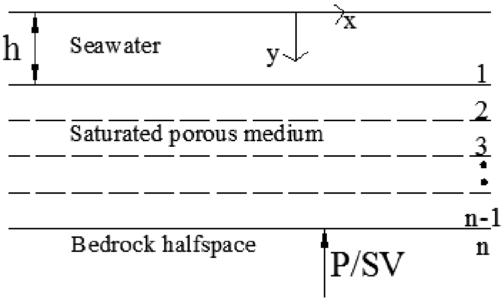

Fig.2 Schematic diagram of free field analysis

2.2 Finite Element Analysis of Inner Domain

When we perform finite element discretization on this area, all the finite element nodes of the entire site calculation area can be divided into three categories: internal nodes, interface points between different media, and artificial boundary points (as shown in Figure 1). The near-field fluctuation problem in the calculation area is controlled by the motion equations of these three types of nodes, which will be introduced separately below.

2.2.1 Motion of internal node

Using the Galerkin method to discretize equations (1) and (2), and considering the influence of boundary conditions, the decoupling motion equilibrium equation of any node i can be obtained as (Chen Shaolin, 2005):

$$\ddot{\mathbf{u}}_i \mathbf{M}_{si} + \mathbf{F}_i^s + \mathbf{T}_i^s - \mathbf{S}_i^s = 0 \tag{4a}$$

$$\ddot{\mathbf{U}}_i \mathbf{M}_{wi} + \mathbf{F}_i^w + \mathbf{T}_i^w - \mathbf{S}_i^w = 0 \tag{4b}$$

Where $\mathbf{M}_{si}$ and $\mathbf{M}_{wi}$ respectively represent the mass of the solid phase and the mass of the liquid phase concentrated at the junction, $\mathbf{F}_i^s$ and $\mathbf{F}_i^w$ respectively represent the solid and liquid constitutive forces concentrated at the nodes, $\mathbf{T}_i^s$ and $\mathbf{T}_i^w$ respectively represent the solid and liquid viscosity resistances concentrated at the nodes, $\mathbf{S}_i^s$ and $\mathbf{S}_i^w$ respectively represent the solid and liquid interface forces acting on the nodes. In the same medium, since all displacements and stresses are continuous, the stresses acting on them through the element interface are equal and opposite directions. In the process of unit assembly, $\mathbf{S}_i^s$ and $\mathbf{S}_i^w$ of the internal nodes are both zero.

If node i is an internal node (non-interface point), At this time, $\mathbf{S}_i^s$ and $\mathbf{S}_i^w$ are equal to zero. If the constitutive relationship is given, the equations (4a) and (4b) can be solved by time-step integration, and the solid and liquid phase displacement recursive formula of node i is finally obtained as follow:

$$\mathbf{u}_i^{(p+1)} = 2\mathbf{u}_i^p - \mathbf{u}_i^{(p-1)} - \frac{(\Delta t)^2}{m_i^s}(\mathbf{F}_i^s + \mathbf{T}_i^s) \tag{5a}$$

$$\mathbf{U}_i^{(p+1)} = 2\mathbf{U}_i^p - \mathbf{U}_i^{(p-1)} - \frac{(\Delta t)^2}{m_i^w}(\mathbf{F}_i^w + \mathbf{T}_i^w) \tag{5b}$$

Where $\mathbf{u}_i^{p+1}$, $\mathbf{u}_i^p$ and $\mathbf{u}_i^{p-1}$ respectively represent the solid phase displacement vectors of node i at time (p+1), p, and (p-1). $\mathbf{U}_i^{p+1}$, $\mathbf{U}_i^p$ and $\mathbf{U}_i^{p-1}$ are the liquid phase displacement vectors of node i at time (p+1), p, and (p-1), respectively. Δt represents the time step, m_i^s and m_i^w are the mass of the solid phase and the mass of the liquid phase concentrated at the *i*-node, respectively.

2.2.2 Motion of interface point

In this section, we discuss the case where node *i* is the interface point of two different saturated porous media, as shown in the figure below.

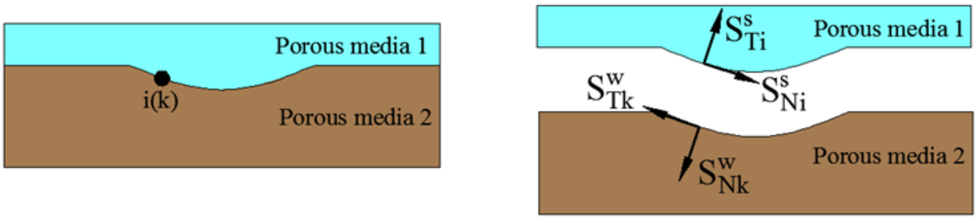

Fig.3 Schematic diagram of interfacial force

If the concept of a separator is used, the dynamic equation of the interface point *i* in medium 1 can be described by (4a) and (4b). The dynamic equation of interface point *k* (the same spatial point as point *i*) in medium 2 is expressed as follows(The physical quantities are underlined to distinguish them from medium 1):

$$\ddot{\bar{\mathbf{u}}}_k \bar{\mathbf{M}}_{sk} + \bar{\mathbf{F}}_k^s + \bar{\mathbf{T}}_k^s - \bar{\mathbf{S}}_k^s = 0 \tag{6a}$$

$$\ddot{\bar{\mathbf{U}}}_k \bar{\mathbf{M}}_{wk} + \bar{\mathbf{F}}_k^w + \bar{\mathbf{T}}_k^w - \bar{\mathbf{S}}_k^w = 0 \tag{6b}$$

By performing time-step integration on the dynamic equation, we can get:

$$\mathbf{u}_i^{(p+1)} = \hat{\mathbf{u}}_i^{(p+1)} + \Delta\mathbf{u}_{Ni}^{(p+1)} + \Delta\mathbf{u}_{Ti}^{(p+1)} \tag{7a}$$

$$\mathbf{U}_i^{(p+1)} = \hat{\mathbf{U}}_i^{(p+1)} + \Delta\mathbf{U}_{Ni}^{(p+1)} + \Delta\mathbf{U}_{Ti}^{(p+1)} \tag{7b}$$

Where

$$\hat{\mathbf{u}}_i^{(p+1)} = 2\mathbf{u}_i^p - \mathbf{u}_i^{(p-1)} - \frac{(\Delta t)^2}{m_i^s}(\mathbf{F}_i^{sp} + \mathbf{T}_i^{sp}) \tag{8a}$$

$$\hat{\mathbf{u}}_i^{(p+1)} = 2\mathbf{u}_i^p - \mathbf{u}_i^{(p-1)} - \frac{(\Delta t)^2}{m_i^s}(\mathbf{F}_i^{sp} + \mathbf{T}_i^{sp}) \tag{8b}$$

$$\Delta\mathbf{u}_{Ni}^{(p+1)} = \frac{(\Delta t)^2}{m_i^s}\mathbf{S}_{Ni}^{sp} \tag{8c}$$

$$\Delta\mathbf{u}_{Ti}^{(p+1)} = \frac{(\Delta t)^2}{m_i^s}\mathbf{S}_{Ti}^{sp} \tag{8d}$$

$$\Delta\mathbf{U}_{Ni}^{(p+1)} = \frac{(\Delta t)^2}{m_i^w}\mathbf{S}_{Ni}^{wp} \tag{8e}$$

$$\Delta\mathbf{U}_{Ti}^{(p+1)} = \frac{(\Delta t)^2}{m_i^w}\mathbf{S}_{Ti}^{wp} \tag{8f}$$

$\Delta\mathbf{u}_{Ni}^{(p+1)}$ is the solid phase displacement caused by the normal interface force $\mathbf{S}_{Ni}^{sp}$, and $\Delta\mathbf{u}_{Ti}^{(p+1)}$ is the solid phase displacement caused by the tangential interface force $\mathbf{S}_{Ti}^{sp}$. $\Delta\mathbf{U}_{Ni}^{(p+1)}$ is the liquid phase displacement caused by the normal interface force $\mathbf{S}_{Ni}^{wp}$, and $\Delta\mathbf{U}_{Ti}^{(p+1)}$ is the liquid phase displacement caused by the tangential interface force $\mathbf{S}_{Ti}^{wp}$.

Similarly, we can get the following formula:

$$\bar{\mathbf{u}}_k^{(p+1)} = \hat{\bar{\mathbf{u}}}_k^{(p+1)} + \Delta\bar{\mathbf{u}}_{Nk}^{(p+1)} + \Delta\bar{\mathbf{u}}_{Tk}^{(p+1)} \tag{9a}$$

$$\bar{\mathbf{U}}_k^{(p+1)} = \hat{\bar{\mathbf{U}}}_k^{(p+1)} + \Delta\bar{\mathbf{U}}_{Nk}^{(p+1)} + \Delta\bar{\mathbf{U}}_{Tk}^{(p+1)} \tag{9b}$$

The terms at the right end of the equal sign are the same as (8).

The continuous conditions of the interface in discrete form are:

$$\mathbf{S}_{Ni}^{s} + \mathbf{S}_{Ni}^{w} = -(\bar{\mathbf{S}}_{Nk}^{s} + \bar{\mathbf{S}}_{Nk}^{w}) \tag{10a}$$

$$\mathbf{S}_{Ti}^{s} = -\bar{\mathbf{S}}_{Tk}^{s} \tag{10b}$$

$$\bar{\beta}\mathbf{S}_{Ni}^{w} = -\beta\bar{\mathbf{S}}_{Nk}^{w} \tag{10c}$$

$$\mathbf{S}_{Ti}^{w} = \bar{\mathbf{S}}_{Tk}^{w} = 0 \tag{10d}$$

$$\mathbf{u}_{Ni} = \bar{\mathbf{u}}_{Nk} \tag{10e}$$

$$\mathbf{u}_{Ti} = \bar{\mathbf{u}}_{Tk} \tag{10f}$$

$$\beta\mathbf{U}_{Ni} = \bar{\beta}(\bar{\mathbf{U}}_{Nk} - \bar{\mathbf{u}}_{Nk}) + \beta\bar{\mathbf{u}}_{Nk} \tag{10g}$$

According to the formulas (7)-(9), and the interface continuous conditions (10), we can get the following formula after derivation(Chen Shaolin, 2019):

$$\mathbf{S}_{Ni}^{sp} = \frac{A_{22}B_1 - A_{12}B_2}{A_{22}A_{11} - A_{12}A_{21}} \tag{11a}$$

$$\mathbf{S}_{Ni}^{wp} = \frac{A_{21}B_1 - A_{11}B_2}{A_{21}A_{12} - A_{11}A_{22}} \tag{11b}$$

where

$$A_{11} = (\Delta t)^2\left(\frac{1}{m_i^s} + \frac{1}{m_k^s}\right) \tag{12a}$$

$$A_{12} = \left(1 - \frac{\bar{\beta}}{\beta}\right)\frac{(\Delta t)^2}{m_k^s} \tag{12b}$$

$$B_1 = \mathbf{n}_i\left(\mathbf{n}_i \cdot \left(\hat{\bar{\mathbf{u}}}_k^{(p+1)} - \hat{\mathbf{u}}_i^{(p+1)}\right)\right) \tag{12c}$$

$$A_{21} = (\Delta t)^2\left(-\frac{\bar{\beta}}{m_k^s} + \frac{\beta}{m_k^s}\right) \tag{12d}$$

$$A_{22} = (\Delta t)^2\left(\frac{\beta}{m_i^w} + \frac{\bar{\beta}^2}{\beta m_k^w} + \frac{\left(\bar{\beta}-\beta\right)\left(\bar{\beta}-\beta\right)}{\beta m_k^s}\right) \tag{12e}$$

$$B_2 = \mathbf{n}_i(\mathbf{n}_i \cdot (\bar{\beta}(\hat{\bar{\mathbf{U}}}_k^{(p+1)} - \hat{\bar{\mathbf{u}}}_k^{(p+1)}) - \beta(\hat{\mathbf{U}}_i^{(p+1)} - \hat{\bar{\mathbf{u}}}_k^{(p+1)}))) \tag{12f}$$

After finding $\mathbf{S}_{Ni}^{sp}$ and $\mathbf{S}_{Ni}^{wp}$ from the formulas (11a) and (11b), we can solve $\bar{\mathbf{S}}_{Nk}^{sp}$ and $\bar{\mathbf{S}}_{Nk}^{wp}$ from the interface continuous condition, according to the continuous condition of solid phase displacement, the following formula can be obtained:

$$\mathbf{S}_{Ti}^{sp} = \frac{\left(\hat{\bar{\mathbf{u}}}_k^{(p+1)} + \Delta\bar{\mathbf{u}}_{Nk}^{(p+1)} - \hat{\mathbf{u}}_i^{(p+1)} - \Delta\mathbf{u}_{Ni}^{(p+1)}\right)m_i^s m_k^s}{(\Delta t)^2(m_i^s + m_k^s)} \tag{13}$$

From formula (10b), we can calculate the interface force $\bar{\mathbf{S}}_{Tk}^{s}$. With the interface force, the displacement response of the interface point can be obtained by formulas (7) and (9).

If the last displacement continuity condition of the saturated bedrock-dry bedrock case in [23] is written as:

$$\beta(\mathbf{U}_{Ni} - \bar{\mathbf{u}}_{Nk}) = 0 \tag{14}$$

After derivation, it can be verified that the calculation formula for this case is a special case of the above formula. Similarly, it can be verified that the above formula is also applicable to the case of fluid-dry bedrock and fluid-saturated bedrock. Therefore, the fluid-structure interaction problem between fluid, saturated bedrock, and dry bedrock can be unified into the same computing framework.

2.3 Motion of artificial boundary node

In order to effectively simulate the motion of the outward traveling wave across the artificial boundary, we use the multiple transmission formula[25]:

$$u_0^{p+1} = \sum_{m=1}^{N} (-1)^{j+1} C_j^N u_j^{p+1-j} \tag{15}$$

Where:

$$C_j^N = \frac{N!}{(N-j)!\,j!} \tag{16}$$

This local artificial boundary condition is universal and has nothing to do with specific wave equations, and can be directly used for wave problems in saturated porous media[26]. Applying formula (15) to the solid-phase and liquid-phase displacements of the saturated porous medium, respectively, the scattered wave field displacements of the boundary point at time p+1 can be obtained, and then add the free field displacement of the boundary point to obtain the total solid and liquid phase displacement of the boundary point.

3. Example analysis

In order to facilitate comparison and verification, the example model in [1] is selected, which is shown in the figure below:

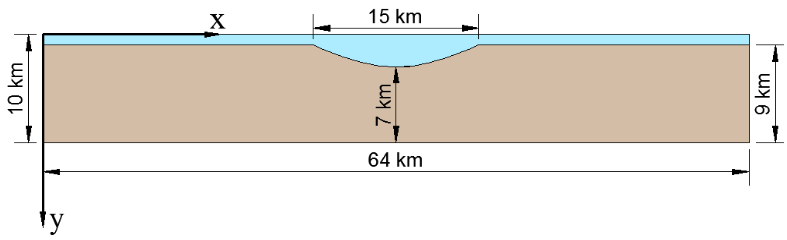

Fig.4 Schematic diagram of computational model

The model is a water-filled cosine-shaped basin with an overlying seawater layer of 1km in thickness. Consider the case where the seabed is bedrock and saturated bedrock, and the relevant material parameters are shown in Table 1. Analyze the response of the model when plane waves are incident vertically. Enter the pulse wave as shown in Figure 5, the time step Δt = 0.0015s, the pulse duration is 4.2s, the number of steps n = 16384, and the calculation time is 24.576s.

Table 1 – Parameters of material

Media	Void ratio /β	μ_0	ρ_s (kg/m^3)	ρ_w (kg/m^3)	ν	G (MPa)	E_w (GPa)	M (GPa)	α	k_0 (μm^2)
Seawater	1	0	0	1000	0.02	0	2.25	2.25	1	1
Saturated bedrock	0.26	0.001	2500	1000	0.188	29.9	2.25	4.78	0.697	10^{-7}
Bedrock	0	0	2500	0	0.188	29.9	0	-	0	0

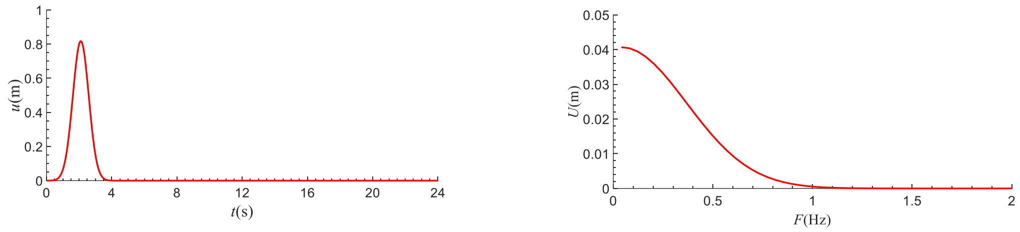

(a) Pulse time history (b) Pulse Spectrum

Fig.5 Input pulse

3.1 Seawater-dry bedrock

Consider seabed as dry bedrock, the displacement wave field of the seabed and dry bedrock under the vertical incidence of pulsed P wave and the response of some points are given. The positions of each point are shown in Figure 6. A_c to E_1 are the points of the seawater layer at the seawater-bedrock interface, and A_2 to I_2 are the points of the bedrock layer at the seawater-bedrock interface.

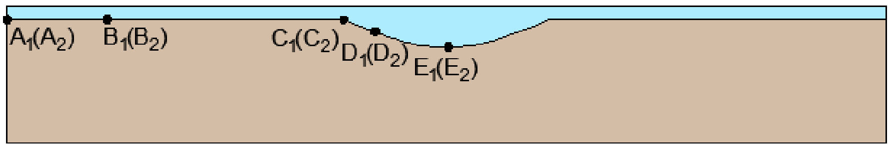

Fig.6 Schematic diagram of observation point

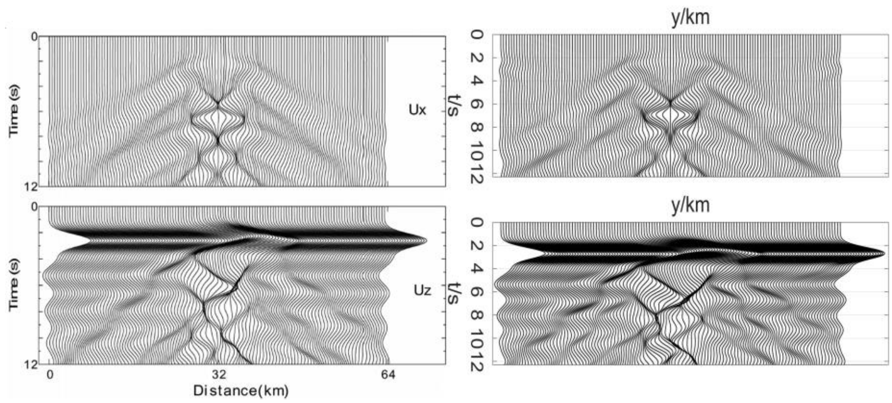

(a) (b)

Fig.7 The displacement at the top of the bedrock layer

Figure 7 shows the horizontal and vertical displacements of the bedrock layer at the seawater-bedrock interface when the P wave is vertically incident. (a) is calculated by Okamoto[1], (b) is calculated by the method in this paper. It can be seen that the waveforms of the two are basically the same, and periodic reflected waves and scattered waves from the depression can be clearly observed at the horizontal part of the sea floor. The surface wave propagating along the interface can also be seen from the figure.

Figure 8 is the wave field diagram of the interface selected when the P wave is vertical incident. U_x^w and U_y^w are the horizontal and vertical displacements of the seawater, u_x^b and u_y^b are the horizontal and vertical displacements of the dry bedrock. It can be seen from the figure that the y-direction displacement is symmetrical about the center point E_1, and the x-direction displacement is antisymmetric about the center point, which is consistent with the result of qualitative analysis. What's more, due to the amplification effect of the free field and the reflection coefficient of the incident wave when it is incident from the seawater to the bedrock is large, the displacement of the seawater surface is large and periodic reflections are formed. The period of the model entering the free vibration phase is 0.267s, which is consistent with the theoretical value $4h/v_p$, h and v_p are the thickness and compression wave velocity of the seawater layer. Comparing Fig. 8 (b) and Fig. 8 (c), the horizontal displacement of the seawater is larger than that of the bedrock. In the flat area, the vertical displacement of the seawater and the bedrock is equal and satisfy the continuous normal displacement, but in the depression area, the seawater has greater displacement.

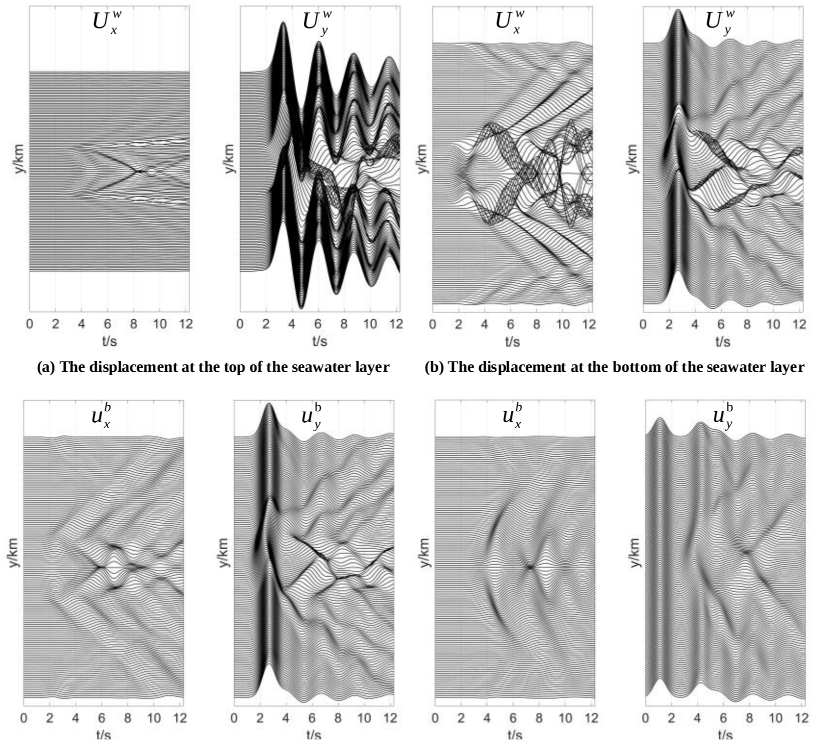

(a) The displacement at the top of the seawater layer **(b) The displacement at the bottom of the seawater layer**

(c) The displacement at the top of the bedrock layer **(d) The displacement at the bottom of the bedrock layer**

Fig.8 Displacement of seawater-bedrock system for P wave incidence

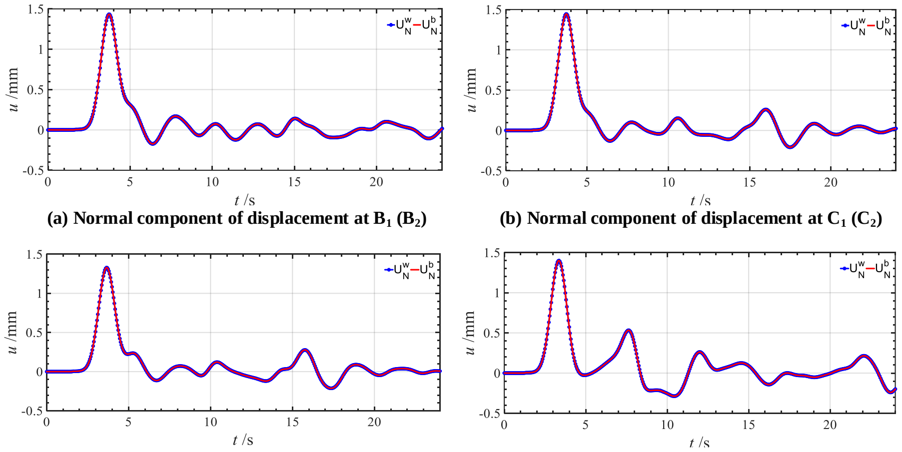

(a) Normal component of displacement at B_1 (B_2) **(b) Normal component of displacement at C_1 (C_2)**

(c) Normal component of displacement at D_1 (D_2) **(d) Normal component of displacement at E_1 (E_2)**

Fig.9 Normal component of displacement on interface in seawater-bedrock system for P wave incidence

Figure 9 shows the normal displacement of the interface point, $\mathbf{U}_N^w$ is the normal displacement of the seawater at the interface, and $\mathbf{U}_N^b$ is the normal displacement of the bedrock at the interface. It can be seen from the figure that $\mathbf{U}_N^w$ and $\mathbf{U}_N^b$ at the same location on the seawater and bedrock interface are completely coincident, satisfying the continuous condition of normal displacement at the seawater-bedrock interface.

3.2 Seawater-saturated bedrock

Considers the seabed as saturated bedrock and analyzes the response of seawater and saturated bedrock under the vertical incidence of pulsed P waves.

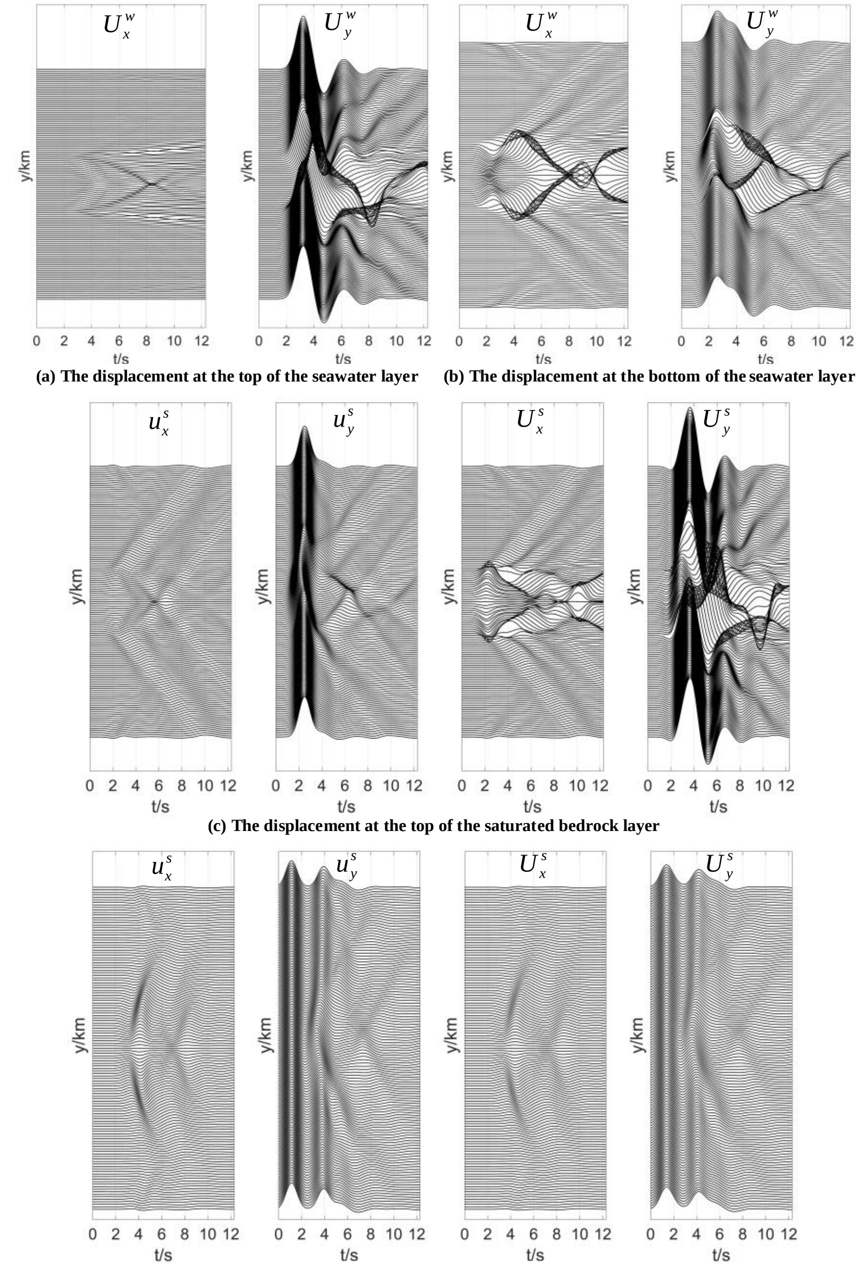

(a) The displacement at the top of the seawater layer (b) The displacement at the bottom of the seawater layer

(c) The displacement at the top of the saturated bedrock layer

(d) The displacement at the bottom of the saturated bedrock layer

Fig.10 Displacement of seawater- saturated bedrock system for P wave incidence

Figure 10 is the wave field diagram of the interface selected when the P wave is vertical incident. u_x^s and u_y^s are the horizontal and vertical solid phase displacements of the saturated bedrock, U_x^s and U_y^s are horizontal and vertical liquid phase displacements of saturated bedrock. Compared with the case where the seabed is dry bedrock, the displacement change of the seawater surface is relatively gentle. This is because the reflection coefficient of the incident wave from seawater to saturated bedrock is smaller than that from seawater to dry bedrock. What's more, viscous damping caused by phase-to-phase relative motion results in faster attenuation. At the interface between seawater and saturated bedrock, the liquid phase displacement of the saturated bedrock is larger than the solid phase displacement, and the waveform is more complicated.

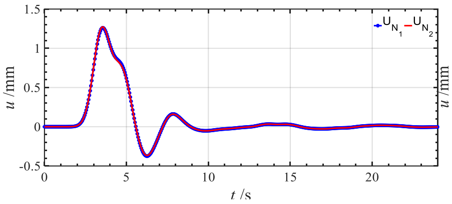

(a) Normal component of displacement at B_1 (B_2)

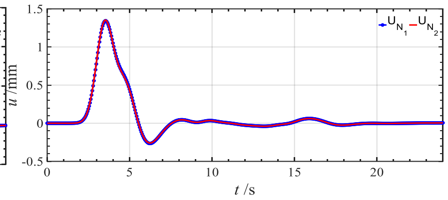

(b) Normal component of displacement at C_1 (C_2)

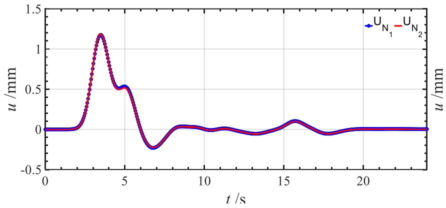

(c) Normal component of displacement at D_1 (D_2)

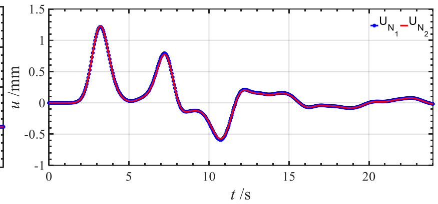

(d) Normal component of displacement at E_1 (E_2)

Fig.11 Normal component of displacement on interface in seawater- saturated bedrock system for P wave incidence

Figure 11 shows the normal displacement at the interface. $\mathbf{U}_{N1}$ is the normal displacement of seawater at the interface, $\mathbf{U}_{N2}$ is the normal displacement of the saturated bedrock at the interface.

$$\mathbf{U}_{N1}=\beta\mathbf{U}_{Ni} \tag{17a}$$

$$\mathbf{U}_{N2}=\bar{\beta}(\bar{\mathbf{U}}_{Nk}-\bar{\mathbf{u}}_{Nk})+\beta\bar{\mathbf{u}}_{Nk} \tag{17b}$$

It can be seen from the figure that $\mathbf{U}_{N1}$ and $\mathbf{U}_{N2}$ at the same position on the interface are completely coincident, which satisfies the continuous condition of normal displacement at the interface (10g).

In summary, the effectiveness of the proposed method is verified by comparison with existing results and by confirmation of the interface continuous conditions.

4. Conclusion

This paper proposes a decoupling simulation technique for near-field fluctuations of seismoacoustic scattering in the sea area when a seismic wave is incident, including free field calculation (providing input for the scattering problem), unified computational framework of fluid-structure interaction in the internal domain, and artificial boundary conditions. The decoupling technology was realized by programming. The responses of the seabed-bedrock sea basin and seawater-saturated sea basin model under vertical incidence of P-wave were analyzed. The effectiveness of the method is verified by comparison with existing results and confirmation of continuous conditions at the interface. This method uses concentrated mass explicit finite element and local transmission artificial boundary, avoids solving large equations, facilitates parallel calculations, has high efficiency, and is suitable for simulation of large-scale marine seismoacoustic scattering problems.

5. Reference

[1] Okamoto, T. , & Takenaka, H. . (1999). A reflection/transmission matrix formulation for seismoacoustic scattering by an irregular fluid-solid interface. *Geophysical Journal of the Royal Astronomical Society*, **139**(2), 531-546.

[2] Qian, Z. H. , & Yamanaka, H. . (2012). An efficient approach for simulating seismoacoustic scattering due to an irregular fluid-solid interface in multilayered media. *Geophysical Journal International*, **189**(1), 524-540.

[3] Ke, X. F. , Chen, S. l. , & Zhang, H. X. . (2018). Freefield analysis of seawater-layered seabed system at P-SV wave incident. *Journal of Vibration Engineering*, **48**(S2), 930-934. (in Chinese)

[4] Takeshi, N. , Hiroshi, T. , Taro, O. , & Yoshiyuki, K. . (2012). FDM simulation of seismic-wave propagation for an aftershock of the 2009 Suruga Bay earthquake: effects of ocean-bottom topography and seawater layer. *Bulletin of the Seismological Society of America*, **102**(6), 2420-2435.

[5] Komatitsch, D. , Barnes, C. , & Tromp, J. . (2000). Wave propagation near a fluid-solid interface: a spectral - element approach. *GEOPHYSICS*, **65**(2), 623-631.

[6] Collins, M. D. , & Siegmann, W. L. . (2017). Treatment of variable topography with the seismoacoustic parabolic equation. *IEEE Journal of Oceanic Engineering*, **42**(2), 488-493.

[7] Tang, J. , Piao, S. C. , & Zhang, H. G. . (2017). Three-dimensional parabolic equation model for seismo-acoustic propagation: theoretical development and preliminary numerical implementation. *Chinese Physics B*, **26**(11), 114301.

[8] Murphy, J. E. , & Chin-Bing, S. A. . (1988). A finite element model for ocean acoustic propagation. *Mathematical and Computer Modelling*, **11**, 70-74.

[9] Biot, & M. A. . (1956). Theory of propagation of elastic waves in a fluid-saturated porous solid. i. low-frequency range. *The Journal of the Acoustical Society of America*, **28**(2), 168.

[10]Biot, M. A. . (1962). Mechanics of deformation and acoustic propagation in porous media. *Journal of Applied Physics*, **33**(4), 1482-1498.

[11]Deresiewicz, H. , & Rice, J. T. . (1964). The effect of boundaries on wave propagation in a liquid-filled porous solid: V. Transmission across a plane interface. *Bulletin of the Seismological Society of America*, **54**(1), 409-416.

[12]Deresiewicz, H. . (1964). The effect of boundaries on wave propagation in a liquid-filled porous solid: VII. Surface waves in a half-space in the presence of a liquid layer. *Bulletin of the Seismological Society of America*, **54**(1), 425-430.

[13]Li, W. H. . (2010). Seismic Response analysis of immersed tube tunnels considering water saturated soil site structure coupling. *Journal of Disaster Prevention and Mitigation Engineering*, **30**(6), 607-613. (in Chinese)

[14]Farhat, C. , & Lesoinne, M. . (2000). Two efficient staggered algorithms for the serial and parallel solution of three-dimensional nonlinear transient aeroelastic problems. *Computer Methods in Applied Mechanics and Engineering*, **182**(3-4), 499-515.

[15]Farhat, C. , Zee, K. G. V. D. , & Geuzaine, P. . (2006). Provably second-order time-accurate loosely-coupled solution algorithms for transient nonlinear computational aeroelasticity. *Computer Methods in Applied Mechanics and Engineering*, **195**(17-18), 1973-2001.

[16]Klaus-Jürgen Bathe, & Zhang, H. . (2004). Finite element developments for general fluid flows with structural interactions. *International Journal for Numerical Methods in Engineering*, **60**(1), 213-232.

[17]Degroote, J. , Haelterman, R. , Annerel, S. , Bruggeman, P. , & Vierendeels, J. . (2010). Performance of partitioned procedures in fluid-structure interaction. *Computers & Structures*, **88**(7-8), 446-457.

[18]Hou, G. , Wang, J. , & Layton, A. . (2012). Numerical methods for fluid-structure interaction - a review. *Communications in Computational Physics*, **12**(2), 337-377.

[19]Habchi, C. , Russeil, S. , Bougeard, D. , Harion, J. L. , Lemenand, T. , & Ghanem, A. , et al. (2013). Partitioned solver for strongly coupled fluid-structure interaction. *Computers & Fluids*, **71**, 306-319.

[20]Mehl, M. , Uekermann, B. , Bijl, H. , Blom, D. , Gatzhammer, B. , & Van Zuijlen, A. . (2016). Parallel coupling numerics for partitioned fluid-structure interaction simulations. *Computers & Mathematics with Applications*, **71**(4), 869-891.

[21]Bungartz, H. J. , Lindner, F. , Gatzhammer, B. , Mehl, M. , Scheufele, K. , Shukaev, A. , & Uekermann, B. . (2016). Precice - a fully parallel library for multi-physics surface coupling. *Computers & Fluids*, **141**, 250-258.

[22]Link, G. , Kaltenbacher, M. , Breuer, M. , & Döllinger, M. . (2009). A 2D finite-element scheme for fluid–solid–acoustic interactions and its application to human phonation. *Computer Methods in Applied Mechanics & Engineering*, **198**(41), 3321-3334.

[23]Chen, S. L. , Ke, X. F. ,& Zhang, H. X. . (2019). A unified computational framework for fluid-solid coupling in marine earthquake engineering. *Chinese Journal of Theoretical and Applied Mechanics*, **51**(2), 1-13. (in Chinese)

[24]Chen, S. L. , Liao, Z. P. ,& Chen, J. . (2005). Decoupling method for near-field wave simulation of two-phase media. *Journal of Geophysics*, **48**(4), 909-917 (in Chinese)

[25]Chen, S. L. , & Liao, Z. P. . (2003). Multi-transmitting formula for attenuating waves. *Acta Seismologica Sinica*, **16**(3), 283-291.

[26]Liao, Z. P. , & Wong, H. L. . (1984). A transmitting boundary for the numerical simulation of elastic wave propagation. *International Journal of Soil Dynamics & Earthquake Engineering*, **3**(4), 174-183.

